Experimental Validation of Global & Local CFD Analysis of Thermoacoustic Refrigerator

Omar Ahmed Al-Mufti[1], Dimitrios Kyritsis[1,2], Isam Janajreh[1,3]
Department of Mechanical & Nuclear Engineering, Khalifa University
Research and Innovation Center on CO2 and Hydrogen (RICH), Khalifa University
Center for Membranes and Advanced Water Technology, Khalifa University
Abu Dhabi, United Arab Emirates
100061896@ku.ac.ae; dimitrios.kyritsis@ku.ac.ae; isam.janajreh@ku.ac.ae

Abstract - In this research, a validated Computational Fluid Dynamics (CFD) analysis of thermoacoustic refrigerator (TAR) is conducted. It is done by firstly simulating the TAR in a global domain (full length resonator and stack) in order to define the flow behaviour near the stack, which is then used to formulate the boundary conditions of the local domain (single plate of the stack). Specifically, the global analysis is performed in order to provide the needed adjacent conditions and to construct higher resolution localized computational domain, thus facilitating parametrical analysis that will then proceed more accurately and swiftly. The experimental setup was developed to validate the broad TAR modelling that considered different stack positions. The experimental results show that optimum frequency decreases when the stack is moved further from the closed end (pressure antinode). The highest temperature difference of 11°C is achieved at normalized stack position of $x_n = 0.33$ and operating frequency of 121 Hz. The experimentally measured speed near the stack differed from the theoretically predicted value by 7 %. The proposed method demonstrated a remarkable level of accuracy in the local analysis, where it predicted the performance of the TAR for all stack positions with maximum error of approximately 2 %.

Keywords: Thermoacoustic refrigeration; CFD; Drive ratio; stack position; TAR operational frequency

1. Introduction

Thermoacoustic is defined as the natural process of conversion of the energy of acoustic waves into thermal energy or vice versa. A thermoacoustic engine (TAE) produces acoustic energy using heat, while a thermoacoustic refrigerator (TAR) converts acoustic energy into a thermal energy by pumping heat from lower temperature reservoir. The acoustic waves can be described as coupled velocity and pressure oscillations [1]. The TAR emerges as an alternative sustainable cooling method when coupled to a TAE that operates on solar/waste heat. This is in addition to the fact that TARs use green gases of zero GWP such as helium, air, and argon. TARs can be classified as standing and travelling wave systems. In a standing-wave system, the pressure and velocity differ in phase by 90°, while in travelling wave systems, they are in phase. Moreover, standing-wave TARs require a stack with poor thermal contact with the fluid, while travelling wave systems require perfect thermal contact in the regenerator. The stack/regenerator is the core component in TAR, which converts the acoustic energy to thermal. This study deals primarily with the standing-wave configuration. The system components schematically illustrated in Figure 1a, comprise the acoustic driver (loudspeaker), heat exchangers, resonance tube, and a stack. The system shown in the figure is closed from both ends (pressure anti-nodes), which implies that this is a half-wavelength ($\lambda/2$) resonator. However, using a quarter-wavelength ($\lambda/4$) resonator is typically preferred because it operates at the same frequency as a half-wavelength ($\lambda/2$) resonator but with half the tube length, which implies less viscous losses [2].

In Figure 1b, we observe a detailed depiction of the thermodynamic cycle within a standing wave TAR. Initially, a gas parcel moves towards the pressure anti-node, leading to compression (A-B). As a result, the parcel undergoes compression and its temperature increases, and consequently becomes hotter than the hot end of the plate. Subsequently, the gas parcel undergoes a heat loss phase (B-C). As it goes back through C-D, it expands, resulting in a decrease in temperature, while displacing towards the velocity anti-node. There, at the cold end of the plate (D), the gas parcel absorbs heat due to its lower temperature. This entire phenomenon, characterized by the transfer of heat from the cold end to the hot end, is referred to as heat pumping or refrigeration.
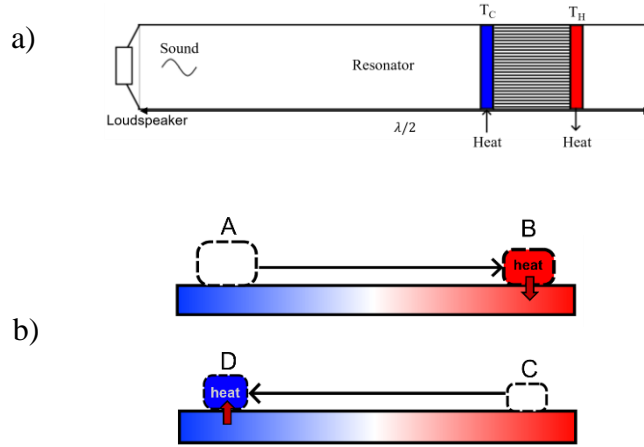
Figure 1: Standing wave TAR schematic (a), and its operating cycle (b)

Computational Fluid dynamics (CFD) analysis of the oscillatory behaviour of TAR systems computes flow parameters such as pressure, temperature, and velocity which is inherently transient at relatively small time steps. To manage computational complexity, an axisymmetric domain is often imposed, albeit at the expense of eliminating secondary rotating flow patterns. Furthermore, a local domain is also possible which considers only a slice of one stack plate pair and a portion of the resonator. This localized approach introduces periodic symmetry in the top/bottom boundary conditions, facilitating higher resolution and accurate computation. Sound wave propagation and interaction within the computational domain are represented by oscillating velocity or pressure, with the other variables calculated based on the imposed conditions. This methodology enables the accurate representation of sound wave behaviour in the TAR system.

Tisovsky and Vit [3] numerically modelled a TAR in a global domain, where the loudspeaker was represented as moving membrane. On the other hand, in the local analysis, the soundwave is replaced by imposing oscillatory boundary at both ends of the domain. Cao et al. [4] suggested that an adiabatic oscillating velocity boundary could simulate the sound wave near the stack at reasonable accuracy. Abd El-Rahman and colleagues [5] employed similar boundary conditions by using a dynamic mesh. However, as per Besnoin [6], at high drive ratios, the velocity boundary condition causes a sustained drift in the computational domain parameters such as the temperature, density, and pressure. Hence, an oscillating pressure was found to be more appropriate at high drive ratios. Other studies, such as that by Rahpeima and Ebrahimi [7], delved into the effects of geometric and thermophysical parameters on TAR performance. It was found that the optimum spacing between plates of the stack is $3.33\delta_k$, i.e. multiple of the thermal penetration depth δ_k which is calculated per Equation 1:

$$\delta_k = \sqrt{2K_g/\omega\rho_m c_p} \qquad (1)$$

Where ρ_m is the mean density, ω is the angular frequency $(2\pi f)$, c_p is specific heat of the fluid, and K_g its thermal conductivity. Zoontjens et al. [8] investigated thermoacoustic couple performance with modified shapes of the plate edges. Aerofoil-shaped edges consistently exhibited the highest temperature differences across all drive ratios. However, in terms of practicality, rounded edges outperformed other shapes. This recommendation is based on their ease of manufacturing and their superior COP. Marx and Blanc-Benon [9] simulated TARs to explore the impact of Mach number and geometrical parameters. Most studies utilize either global or local domains individually. In this study, a method of synergistically using the two domains is proposed to achieve an accurate simulation of the TAR performance with a reasonable computational complexity.

2. Methodology

The current study comprises two stages, the first is simulating the TAR in a global domain to identify the flow characteristics near the stack. This will aid in defining the boundary conditions of the local-analysis domain, which is the second stage. The results from local analysis will be compared with experiments to validate the model accuracy.

The flow is modelled as a compressible flow of an ideal gas equation that is governed by the three conservative laws, i.e. the mass/continuity, momentum, and energy equations, representing a complete set of the Navier-stokes equations as given below:

$$\frac{\partial \rho}{\partial t} + \nabla.(\rho \vec{V}) = 0 \tag{2}$$

$$\left[\frac{\partial(\rho \vec{V})}{\partial t} + \nabla.(\rho \vec{V}\vec{V})\right] = -\nabla p + \nabla.\mu[(\nabla\vec{V} + \nabla\vec{V}^T) - \frac{2}{3}\nabla.\vec{V}I] + \rho\vec{g} \tag{3}$$

$$\frac{\partial(\rho E)}{\partial t} + \nabla.\left(\rho\vec{V}(\rho E + p)\right) = -\nabla.\left[K\nabla T + \left(\mu(\nabla\vec{V} + \nabla\vec{V}^T) - \frac{2}{3}\nabla.\vec{V}I\right)\vec{V}\right] \tag{4}$$

Where $\vec{V}$ corresponds to the velocity vector, ρg represents the gravitational body forces, E is the internal energy, K is the thermal conductivity. Internal energy has the form $E = H - p/\rho + \frac{1}{2}\vec{V}.\vec{V}$ with H representing the enthalpy of the system and is thermodynamically expressed using the static temperature (T) and specific heat (c_p) of the fluid medium, i.e., $H = c_p(T - T_o)$ $with$ $T_o$is the reference temperature. In thermoacoustic systems, turbulence should be considered at drive ratios as low as 0.45%. Where drive ratio is defined as per Equation 5:

$$D = \frac{p_0}{p_m} \tag{5}$$

Where p_0 is the pressure amplitude at pressure anti-node, and p_m is the mean pressure The drive ratio in the current study is around 1.5 %. Thus, turbulence was modelled using the standard k-ε model, which is widely used and validated for various thermoacoustic problems in the literature [10-12]. The general transport equation following the common eddy viscosity model is given in Equation 6 as:

$$\frac{\partial(\rho\emptyset)}{\partial t} + \nabla.\left(\rho\vec{V}\emptyset - \Gamma\nabla\emptyset\right) = S_{\emptyset_k} \tag{6}$$

Where $\emptyset$ can represent either the turbulence kinetic energy (k) or the dissipation rate (ε), Γ is the diffusion coefficient and S is a source term related to k or ε.

Figure 2a depicts the global axisymmetric computational domain which stretches 550 mm length and 35 mm radius. The mesh has 177,575 elements that are predominantly quadratic. It is refined near the stack where the thermoacoustic effect occurs and is iteratively discretized to achieve near normalized wall distance of y+=1 to resolve the viscous sublayer. The axis of symmetry implies that the stack is spiral and with a blockage ratio of 0.8 and spacing between the spirals is 1.1 mm, where blockage ratio is defined as:

$$B = \frac{h}{y + h} \tag{7}$$

In which h is the plate/spiral thickness, and y is the spacing between spirals/plates. Figure 2b shows the local domain which is just a subset of the global domain that comprises a discretized mesh of 64773 elements. The top and bottom

boundaries are conformal periodic pairs, and the sound wave is simulated via moving walls (dynamic mesh). The moving walls were positioned at a distance of 0.0085λ from the stack ends [4].
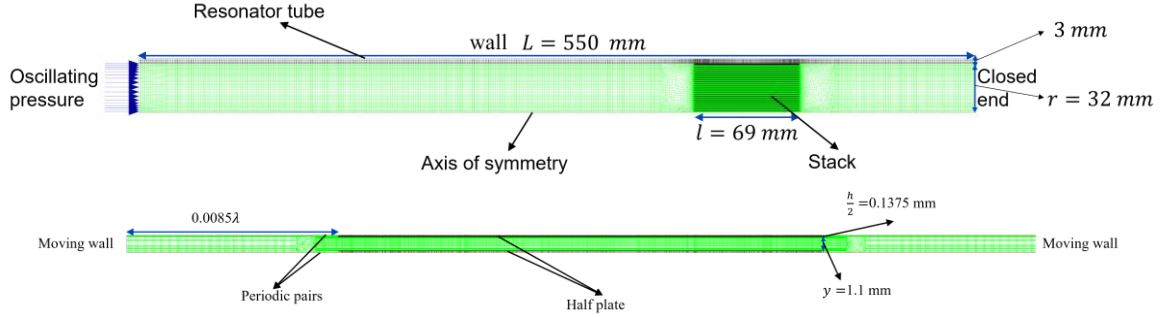

Figure 2: a) Global & b) Local computational domains

As for the boundary conditions, the inlet of global domain was set as oscillating pressure as:

$$p = p_0 cos(kx_{inlet})sin(\omega t) \tag{8}$$

Where t is the time, x_{inlet} is the distance of the inlet from the closed end (550 mm), and k is the wave number:

$$k = \frac{\omega}{a} \tag{9}$$

In which a is the speed of sound of the fluid. p_0 and operating frequency (f) were provided by experimental data. In the local domain, the oscillating walls move with speed u given by:

$$u = u_{wall}\cos(\omega t) \tag{10}$$

Where u_{wall} is the velocity amplitude at the moving wall position determined from the global analysis. Similarly, the temperature of the moving wall was set to be oscillating as described by Equation 11:

$$T = T_{m,wall} + \frac{p_0}{\rho_m c_p}\sin(\omega t) \tag{11}$$

Where $T_{m,wall}$ is the mean temperature over the positions of the oscillating wall, inferred from the global analysis. In both domains, conjugated heat transfer and no-slip ($u = 0$) boundary conditions were imposed at the stack walls. The temperature gradient along the stack was initially set same as the one measured experimentally to facilitate faster convergence. Furthermore, the stack is made of castable wax-resin which has a density of 1110 kg/m³, a heat capacity of 1350 J/kg.K, and a thermal conductivity of 0.3W/m.K [13,14], while the resonator is made of plexiglass which has a density of 1190 kg/m³, heat capacity of 1500 J/kg.K, and a thermal conductivity of 0.189 W/m.K. Initially, the temperature is 22°C and the pressure is 1 atm.

The simulations were done using Ansys Fluent following the SIMPLE pressure-velocity coupling solver. All variables were discretized using 2nd order, i.e., upwind for spatial and central for time derivatives. To capture the thermoacoustic effects, the time step is minimized that adhere to the CFL < 1 constrains with a uniform value of 5e-5 s.

2.1. Experimental setup development

Figure 3 illustrates a schematic of the developed TAR experimental setup showing system components and their connections. The function generator (KEITHLEY 3390 50MHz, Taiwan) produces a sinusoidal wave that is amplified (LF-05T amplifier) and connected to the loudspeaker (Kenwood KFC-S1066, China). The loudspeaker is attached to the resonator

tube using a reducer cone. This arrangement mimics an open-end on the speaker side, and hence a quarter wavelength configuration. The resonator is made of plexiglass tube of 550 mm long and 64 mm inner diameter. The other end of the resonator is sealed using a 3D printed cap. The pressure at closed end was measured using a sound level meter (Quest 2200R, USA, accuracy: $\pm$ 0.7 dB, calibrated using QC-10 calibrator) with a sealed protruding microphone stem through a 12.7 mm hole in the end cap. The oscilloscope (TEKTRONIX TDS3034C, China) is used to measure the voltage fed to the speaker and ensure that the signal remained sinusoidal without any clipping. For temperature measurements, three Omega K-type thermocouples (accuracy: $\pm$ 0.25 %, calibrated using Omega CL134) are used to record the mean, the hot, and cold end temperatures. The thermocouple signals are read through NI 9211 module which is attached to NI cDAQ-9178 data acquisition chassis and connected to PC/Labview. The stack is 3D printed and is made of a castable wax-resin, which has a low thermal conductivity (~0.3 W/m.K) and with the same dimensions that described in the numerical model. The experiments were carried out at six positions along the stack, specifically at 5, 10, 15, 25, 35, and 45 cm. These positions correspond to the distance from the closed end (pressure antinode) to the center of the stack. At each position, frequencies in the range of 90 -165 Hz were tested to find the optimum frequency (i.e., the frequency that achieves the highest temperature difference). The performance was evaluated based on the obtained temperature difference between the hot and cold ends. Moreover, and following [2,15], the stack position and length were normalized in the results as:

$$x_n = kx \tag{12}$$

$$l_n = kl \tag{13}$$

Where k is the wave number, and x and l are respectively the stack center position (measured from the closed end) and the stack length both expressed in m.
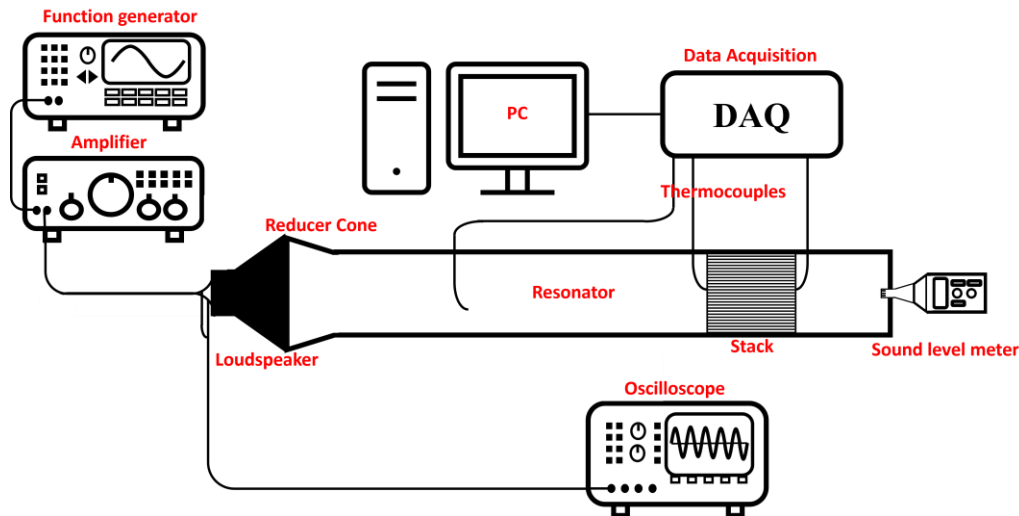

Figure 3: Experimental setup components and connections

3. Results and discussion

Experientially, the highest pressure amplitude measured at the closed end of approximately 1,500 Pa and it occurred at frequency in the range of 105 Hz to 126 Hz, depending on the stack position. The TAR is expected to have the optimum performance in this range of frequencies. Figure 4a shows the obtained temperature difference vs frequency for different stack positions. The highest temperature difference of 11°C occurred at 121 Hz and when the stack center was positioned 15 cm away from the closed end. It can also be noticed that the optimum frequency decreased when the stack was moved away from the closed end. This agrees with the Alamir's results in [16]. Furthermore, Figure 4b shows the temperature

evolution of the optimum case (15 cm at 121 Hz). The mean temperature remained almost unchanged. The hot and cold ends temperatures dispersed most during the first 500 seconds then asymptotically reached their equilibrium values. This optimum case (15 cm at 121 Hz) corresponds to a normalized position of $x_n = 0.33$, noting that the normalized stack length is $l_n = 0.151$.
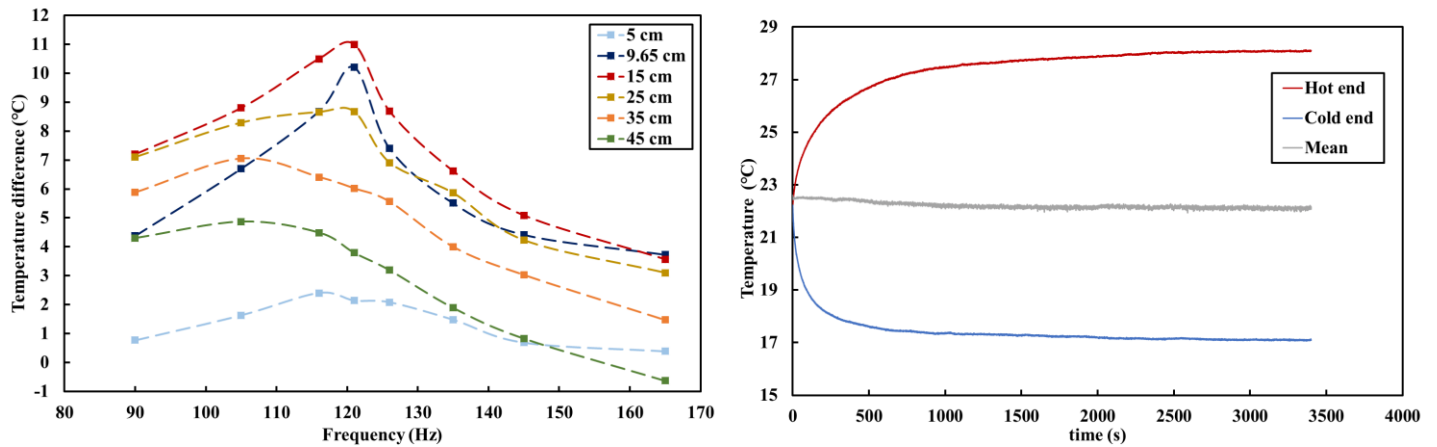

Figure 4: a) Temperature difference vs frequency for different stack positions and b) Evolution of temperatures for a stack at normalized position of 0.33

Results of the global analysis are presented in Figure 5a, which depicts the attained quasi-steady pressure at the closed end over one acoustic cycle and reaching to 1,500 Pa. This attained value is approximately in close match to the experimentally measured value (1501.568 Pa), which highlights the accuracy of the imposed boundary condition (Equation 8). As for the flow characteristics, when the stack is positioned at $x_n = 0.33$, the velocities at the locations of moving walls in the local analysis are 0.674 m/s of the closed end and 1.537 m/s at the open end. These values are slightly different than the theoretical values ($u = \frac{p_0}{\rho_m a} cos(kx_{wall})$) which are 0.683 m/s & 1.661 m/s. The discrepancy is larger at the position of higher velocity reaching 7% of relative error. T the mean temperature at these localized positions are 24°C and 20°C near the hot and cold end, respectively.

In the local numerical analysis, convergence is achieved when the change in temperature gradient is less than 0.002% between two successive acoustic cycles. Figure 5b depicts a comparison between the measured experimental data and those obtained numerically from the local analysis. Evidently, the numerical model was able to accurately predict the performance of the TAR at different stack positions. This again, is attributed to accurate boundary conditions imposed on the local domain that were inferred from the global model. On the other hand, assuming adiabatic oscillating walls per the work of Cao et al. [4], would lead to a large discrepancy in these results. Such an assumption would be more appropriate for a well-insulated system. Obtaining such accurate results from a localized CFD analysis holds substantial importance, becausethe localized domain provides an instrumental tool in order to carry out exhaustive parametrical analysis at low computational cost.
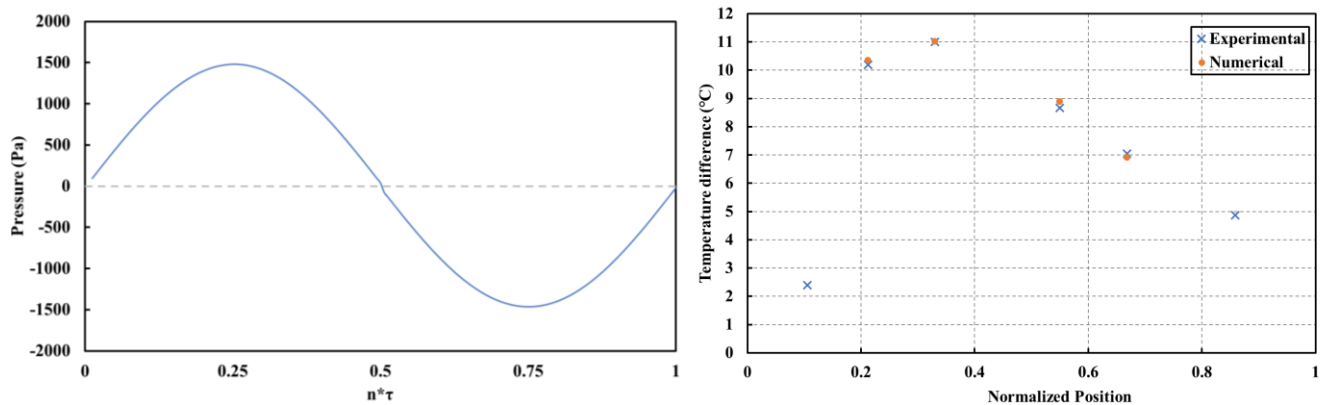
Figure 5: a) Total pressure at the closed end during one acoustic cycle ($\tau = \frac{1}{f}$) and b) Numerical and Experimental temperature difference for different stack positions

4. Conclusion

In this study, CFD analysis of the global and the local thermoacoustic refrigerator (TAR) was done. Because the global analysis of TARs is computationally costly and carried at lower resolution, it has been shown that is useful to perform the computation by creating a local subdomain and assigning accurate boundary conditions that feed in from the global analysis. The proposed method was validated against experimental results at different stack positions. The system ran on a drive ratio of approximately 1.5%. It achieved the highest temperature gradient of 11°C when the stack normalized position was $x_n = 0.33$ and at frequency of 121 Hz. The numerical model showed high accuracy in terms of predicting the temperature distribution along the stack for all positions, with a maximum error of around 2%. An accurate local domain model is extremely useful, as it takes less time and computational resources thus allowing further sensitivity analysis. Based on these conclusions, future work will include validating the model at high drive ratios and conducting further sensitivity analysis.

References

[1] G. W. Swift, *Thermoacoustics*. Cham: Springer International Publishing, 2017. doi: 10.1007/978-3-319-66933-5.

[2] M. E. H. Tijani, "Loudspeaker-driven thermo-acoustic refrigeration," 2001.

[3] T. Tisovsky and T. Vit, "Design of numerical model for thermoacoustic devices using OpenFOAM," Pilsen, Czech Republic, 2017, p. 020043. doi: 10.1063/1.5004377.

[4] N. Cao, J. R. Olson, G. W. Swift, and S. Chen, "Energy flux density in a thermoacoustic couple," *The Journal of the Acoustical Society of America*, vol. 99, no. 6, pp. 3456–3464, Jun. 1996, doi: 10.1121/1.414992.

[5] Abd El-Rahman and E. Abdel-Rahman, "Computational Fluid Dynamics Simulation of a Thermoacoustic Refrigerator," *Journal of Thermophysics and Heat Transfer*, vol. 28, no. 1, pp. 78–86, Jan. 2014, doi: 10.2514/1.T4150.

[6] E. Besnoin, "Numerical Study of Thermoacoustic Heat Exchangers," 2001.

[7] R. Rahpeima and R. Ebrahimi, "Numerical investigation of the effect of stack geometrical parameters and thermo-physical properties on performance of a standing wave thermoacoustic refrigerator," *Applied Thermal Engineering*, vol. 149, pp. 1203–1214, Feb. 2019, doi: 10.1016/j.applthermaleng.2018.12.093.

[8] L. Zoontjens, C. Q. Howard, A. C. Zander, and B. S. Cazzolato, "Numerical comparison of thermoacoustic couples with modified stack plate edges," *International Journal of Heat and Mass Transfer*, vol. 51, no. 19–20, pp. 4829–4840, Sep. 2008, doi: 10.1016/j.ijheatmasstransfer.2008.02.037.

[9] D. Marx and P. Blanc-Benon, "Computation of the temperature distortion in the stack of a standing-wave thermoacoustic refrigerator," *The Journal of the Acoustical Society of America*, vol. 118, no. 5, pp. 2993–2999, Nov. 2005, doi: 10.1121/1.2063087.

[10] G. Yu, W. Dai, and E. Luo, "CFD simulation of a 300Hz thermoacoustic standing wave engine," *Cryogenics*, vol. 50, no. 9, pp. 615–622, Sep. 2010, doi: 10.1016/j.cryogenics.2010.02.011.

[11] G. Chen, L. Tang, Z. Yu, and B. Mace, "Mode transition in a standing-wave thermoacoustic engine: A numerical study," *Journal of Sound and Vibration*, vol. 504, p. 116119, Jul. 2021, doi: 10.1016/j.jsv.2021.116119.

[12] O. Al-Mufti and I. Janajreh, "Single plate analysis of thermoacoustic refrigerator," *International Journal of Thermal and Environmental Engineering*, 2023.

[13] A. Oval-Trujillo, A. Rodríguez, G. Pérez-Artieda, Y. Dung, and P. Alegría, "Experimental measurement of thermal conductivity of stereolithography photopolymer resins," *SN Appl. Sci.*, vol. 4, no. 8, p. 205, Aug. 2022, doi: 10.1007/s42452-022-05087-9.

[14] J. M. Ashraf, S. E. Taher, D.-W. Lee, K. Liao, and R. K. Abu Al-Rub, "On the computational modeling, additive manufacturing, and testing of tube-networks TPMS-based graphene lattices and characterizing their multifunctional properties," *APL Materials*, vol. 10, no. 12, p. 121107, Dec. 2022, doi: 10.1063/5.0101412.

[15] J. R. Olson and G. W. Swift, "Similitude in thermoacoustics".

[16] M. A. Alamir, "Experimental study of the stack geometric parameters effect on the resonance frequency of a standing wave thermoacoustic refrigerator," International Journal of Green Energy, vol. 16, no. 8, pp. 639–651, Jun. 2019, doi: 10.1080/15435075.2019.1602533.